Composite Structures 137 (2016) 148–158

Contents lists available at ScienceDirect

Composite Structures

journal homepage: www.elsevier.com/locate/compstruct

Predicting matrix failure in composite structures using a hybrid failure criterion

Nayeem Tawqir Chowdhury [a,*], John Wang [b], Wing Kong Chiu [a], Wenyi Yan [a]

[a] Department of Mechanical and Aerospace Engineering, Monash University, Clayton, VIC 3800, Australia
[b] Aerospace Division, Defence Science and Technology Group, 506 Lorimer St., Fishermans Bend, VIC 3207, Australia

ARTICLE INFO

Article history:
Available online 14 November 2015

Keywords:
Matrix failure
Composites
Four-point bending test
Truncation
Failure envelope

ABSTRACT

Matrix failure in composite structures has not been widely presented in literature. Their failure has often been overlooked due to focus directed at fiber failure. With increasing attention on progressive damage models for composite structures it is important that matrix failure is well understood as this is often the characteristic of initial failure in these advanced materials. In this paper the authors perform several four point bend tests on a typical stacking sequence used in composite structures $[-45/0/45/90]_{2S}$. Inspection techniques involving a FLIR thermal camera are used to detect matrix failure. Two methods are then employed to establish a suitable failure criterion to predict matrix failure. The first compares several failure criteria at the lamina level, whilst the second uses micromechanical analysis to predict matrix failure. It was found that matrix failure was poorly predicted at the lamina level, whilst a hybrid failure criterion incorporating the 1st Stress Invariant and Drucker–Prager failure criterion at the micromechanical level gave a much better prediction. The proposed hybrid failure criterion can be used in various progressive damage models to give a better prediction of initial failure in composite structures.

1. Introduction

Composite materials are increasingly being used due to their high strength to weight ratio and high fatigue resistance. Their extensive use can be found in the recently developed military helicopters such as the Eurocopter Tiger and Bell/Boeing V22 where the airframe is made of nearly all composites. In order to ensure structural integrity in such applications, it is important to understand the material behavior at failure. However as failure in composites are characterized by different modes, namely fiber, matrix and interfacial failure [1], this has complicated their understanding. For this reason there are still many unanswered questions as to the materials' failure characteristics, one such area includes matrix failure.

Conventional laminate theory (CLT) is widely used to model composite structures [2]. CLT uses an averaging approach to combine the properties of the matrix and fiber to form what is considered to be a new homogeneous material called a lamina. The advantage of using this theory is that it is simple to use and does a good job in predicting ply failure [2]. With advances in computing resources available in industry it has been possible to extend CLT and establish a more detailed model, although modeling each strand of fiber embedded in a matrix material is still considered computationally prohibitive. One such method that is gaining popularity is micromechanical analysis where the homogenous material created using CLT is broken back down to its individual constituents using Representative Volume Elements (RVEs). Multicontinuum theory (MCT) is one of these methods [1,3].

With these advances, it has meant that further research is required to understand the behavior of the individual constituents that make up the laminate rather than stopping at the lamina level. This is where matrix failure in composites plays an important role. Despite being one of the constituents in a composite it's behavior has often been overlooked as the behavior of the fiber constituent is usually the most visible form of failure in composite structures [4,5] and often detectable on a load–displacement curve. Conversely, matrix failure is often not very visible and hard to pick up on a load–displacement curve [6]. Even if picked up on a curve it is difficult to pinpoint the location in the laminate. By establishing an experiment method that is able to pinpoint matrix failure, various matrix failure criteria can be tested for their accuracy. Once a suitable failure criterion is selected, it can be used in progressive damage models which have been gaining large interest quite recently [7–11]. In this paper the authors use a Forward-Looking Infrared Radar (FLIR) thermal imaging camera to aid in detecting failure alongside visual inspection post failure detection.

* Corresponding author.
E-mail address: nayeem.chowdhury@monash.edu (N.T. Chowdhury).

http://dx.doi.org/10.1016/j.compstruct.2015.11.019
0263-8223/

In this paper the authors perform several four point bend tests on a laminate with a typical stacking sequence of $[-45/0/45/90]_{2S}$. The results are used to compare several well-known failure criteria [4] to predict failure of the matrix at the lamina level using CLT. The analysis method is then extended to perform micromechanical analysis where the failure criterion proposed by the authors in two previous investigations [12,13] is used for comparison purposes. In those investigations biaxial tensile tests on fiber reinforced polymer composite (FRPC) specimens and neat resin specimens were performed on the same matrix material discussed in this paper (EP280) [14]. The proposed stress based failure criterion for the matrix is tested for its validity in this paper.

The paper starts with presenting the experimental setup and results. Then the two analysis methods are described in Sections 3 and 4 followed by a final discussion comparing the prediction of the two analysis methods.

2. Experiments

2.1. Experiment setup

The experiments were performed using a four point bend test fixture. The procedure outlined in ASTM D7264 [15] was followed. The material used is called EP280 Prepreg [14], with material properties presented in Table 1. The specimen layup consisted of 16 plies with a symmetric stacking sequence given by $[-45/0/45/90]_{2S}$. The dimensions and material coordinate system are shown in Fig. 1. A plate made up of the prepreg material was cured in an autoclave at 120 °C for 60 min with a ramp up rate of 2 °C/min. Care was taken to ensure that the fiber directions were aligned correctly. The specimens were machined from the cured plate using a CNC milling machine. Final machining of the specimen sides was performed on a diamond wheel to minimize damage from the milling process.

In total 8 specimens were tested on a 5 kN Instron test machine. The span between the two bottom supports and the two top supports were 128 mm and 64 mm respectively. A loading rate of 4 mm/min was used resulting in failure taking place at 3–5 min from the start of loading.

Four of the eight specimens tested had strain measurements recorded. Instead of using a conventional strain gauge, strain was measured along the length of the specimen by bonding a fiber optic cable [16,17] in the thickness of the specimen as shown in Fig. 2. The advantage of using the fiber optic cable to measure the strain is that the relative size (width) of the specimen to a strain gauge is smaller so a more localized strain in our experiments can be compared against our FE model.

In conjunction with the strain measurement, a FLIR thermal imaging camera was used to capture any thermal spikes that result from failure of the specimen. However this technique is only able to observe failure on exposed faces of the specimen and cannot capture any internal damage or damage on surfaces that aren't facing the view of the camera.

Table 1
Prepreg material properties.

Property	
E11	131 GPa
E22	6.20 GPa
E33	6.20 GPa
v12	0.28
v23	0.40
v13	0.28
G12	4.73 GPa
G23	1.44 GPa
G13	4.73 GPa

2.2. Experiment results

The time at failure picked up by the FLIR thermal camera was used as the basis for analyzing the results. Fig. 3 shows an example of the temperature spike picked up by the FLIR camera for specimen 2. Table 2 records the displacements at failure for the 8 experiments performed.

From Table 2 it can be seen that the overall consistency of the observed point at failure was good with a standard deviation of 0.90 mm and mean of 7.66 mm.

3. Method 1: failure at the lamina level

3.1. Finite element analysis

Finite element analysis was used to process all the experimental results to establish which ply had failed and to obtain the stress and strain states on the matrix. The finite element package ABAQUS 6.13 was used [18]. Each of the 16 plies were modeled with 4 elements through their thickness. The top and bottom nodes of each ply were tied together to assume a perfect contact. 8-node linear brick elements with reduced integration and hourglass control were used for the specimen (C3D8R) [18]. In total there were 39168 elements and 46865 nodes. The material properties listed in Table 1 were assigned to each Ply with an orientation specified through ABAQUS GUI. A frictionless tangential constraint was applied between the top loading pins and the specimen whilst a zero displacement constraint along the x-direction was applied in the positions of the bottom supports. Fig. 4 shows the boundary conditions applied to the FE model.

The strain along path AA (ε_x) shown in Fig. 4 was extracted and plotted in Fig. 5. These strains were extracted from 4 of the experiments (specimens: 5–8) at 100s from the start of loading. The corresponding displacements at this time were used in the FEA models to obtain a comparative strain state. Our FEA model matched our experiment values to within 10%, thus it was considered appropriate for the remainder of the analysis.

3.2. Results

The strain state (along path BB) of the specimen shown in Fig. 5, is extracted for each ply and is shown in Tables 3 and 4. The inner plies were found to experience lower order values and were not considered to fail before any of the four outer plies. They are excluded for the remainder of this analysis.

3.3. Failure Prediction at the Lamina Level

Conventional analysis techniques have usually stopped at the laminae level [4,19,20]. To provide an idea of predicting matrix failure at this level, various failure criteria are compared. The following criteria are considered:

1. Maximum Stress failure criterion.
2. Maximum Strain failure criterion.
3. Tsai–Hill's failure criterion.
4. Tsai–Wu's failure criterion.
5. Hashin–Rotem failure criterion.

These lamina level failure criteria require information about the stresses at failure for the lamina (EP280 Prepreg) used in this investigation. Thus, several experiments were performed on the lamina material to obtain its critical failure stresses which are shown in Table 5. Where 'F_{ij}' is the critical failure stress, 'i' is the material direction and 'j' represents whether the stress is

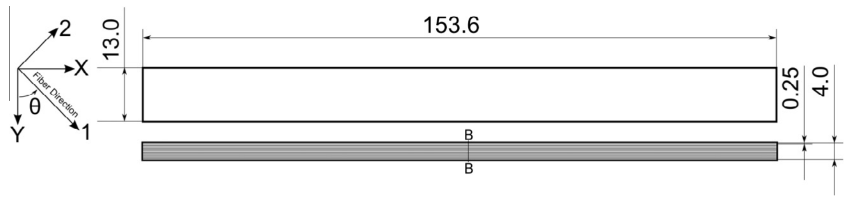

Fig. 1. Four point bend specimen dimensions.

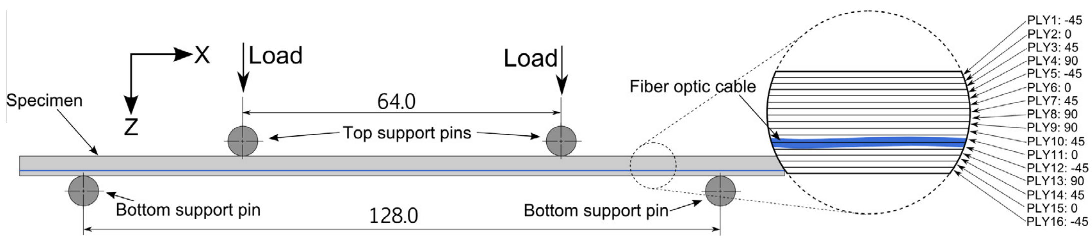

Fig. 2. Experimental setup of the 4 point bend test.

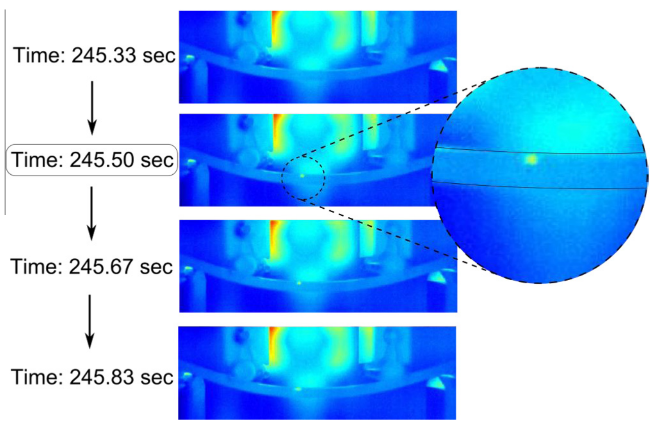

Fig. 3. Temperature spike picked up at failure in Test 2.

Table 2
Displacement at failure for the 8 specimens tested.

Specimen	*Displacement applied at initial failure (mm)*
1	7.61
2	7.18
3	7.39
4	6.80
5	8.79
6	9.29
7	6.97
8	7.24

compressive (c) or tensile (t). F_4, F_5, and F_6 are the critical failure stresses for σ_{23}, σ_{13}, and σ_{12} respectively. The experiments involved: longitudinal tensile tests, transverse tensile tests and transverse compressive tests performed in accordance with the ASTM D3039 and ASTM D695 standards, respectively [21,22]. In-plane and out-of-plane shear tests were also performed in accordance with ASTM D5379 [23]. The stress/strain behaviors are shown in Fig. 6.

From Fig. 6 it can be seen that the material demonstrated non-linearity in shear whilst behaving linearly under normal loading. In order to capture this behavior; the critical failure strains shown in Table 4 are converted to stresses using the concept of a linear stress strain behavior in the material normal directions and nonlinear material behavior in the shear directions (from Fig. 6). Note that shear in the '13' direction is assumed to be the same as in the '12' directions [24]. As matrix failure is the primary interest of this paper, ply 2 and 15 are excluded from the remainder of this investigation as their behavior is predominantly influenced by the fiber. The stress based failure results are presented in Table. 6.

3.3.1. Maximum stress failure criterion

Maximum stress failure theory is given by Eqs. (1)–(6) in a failure index form, where a value greater than 1 indicates failure. σ_{11}, σ_{22}, σ_{33} are the stresses in the longitudinal (fiber), transverse and out-of-plane directions respectively. σ_{12}, σ_{13}, σ_{23} are the two in-plane shear stress and one out-of-plane shear stress values respectively. F_{ij} is the critical failure stresses of the lamina given in Table 5, where the subscript '*i*' denotes the material direction and subscript '*j*' represents whether the failure is tensile (t) or compressive (c) in nature. The results for each Ply are shown in Table 7.

$$\left.\begin{array}{ll} \text{when } \sigma_{11} > 0 & \frac{\sigma_{11}}{F_{1t}} \\ \text{when } \sigma_{11} < 0 & \frac{\sigma_{11}}{-F_{1c}} \end{array}\right\} = 1 \tag{1}$$

$$\left.\begin{array}{ll} \text{when } \sigma_{22} > 0 & \frac{\sigma_{22}}{F_{2t}} \\ \text{when } \sigma_{22} < 0 & \frac{\sigma_{22}}{-F_{2c}} \end{array}\right\} = 1 \tag{2}$$

$$\left.\begin{array}{ll} \text{when } \sigma_{33} > 0 & \frac{\sigma_{33}}{F_{3t}} \\ \text{when } \sigma_{33} < 0 & \frac{\sigma_{33}}{-F_{3c}} \end{array}\right\} = 1 \tag{3}$$

$$\frac{|\sigma_{23}|}{F_4} = 1 \tag{4}$$

$$\frac{|\sigma_{13}|}{F_5} = 1 \tag{5}$$

$$\frac{|\sigma_{12}|}{F_6} = 1 \tag{6}$$

3.3.2. Maximum strain failure criterion

Maximum strain failure criterion [4] is presented in its stress form given by Eqs. (7)–(12). The results for each Ply are shown in Table 8.

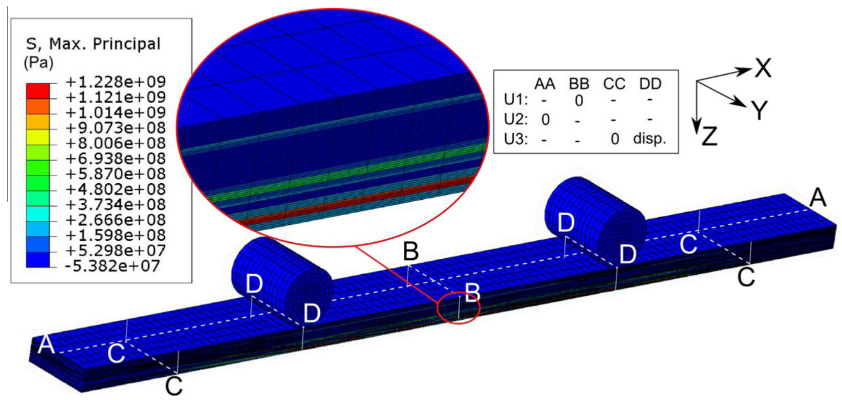

Fig. 4. FEA model of the specimen along with boundary conditions. Where: displacement in the *x*, *y*, *z* directions is denoted as U1, U2, U3 respectively. 'disp' is the displacement values taken from Table 2.

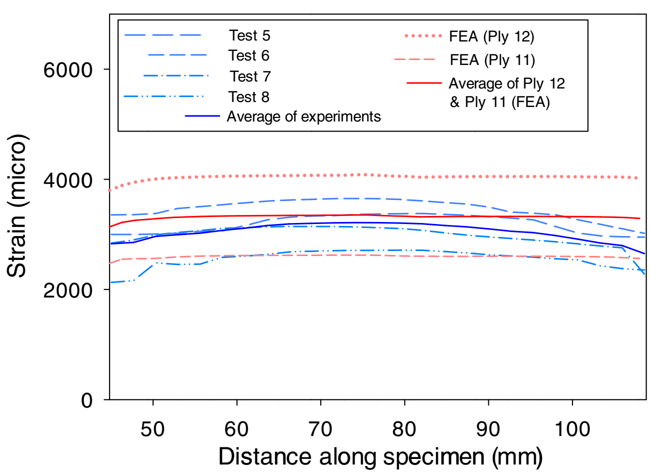

Fig. 5. Comparison of the FEA and experiment strain values at a time of 100 s.

$$\left.\begin{array}{ll} \text{when } \epsilon_{11} > 0 & \frac{\sigma_{11}-\upsilon_{12}\sigma_{22}-\upsilon_{13}\sigma_{33}}{F_{1t}} \\ \text{when } \epsilon_{11} < 0 & \frac{\sigma_{11}-\upsilon_{12}\sigma_{22}-\upsilon_{13}\sigma_{33}}{-F_{1c}} \end{array}\right\} = 1 \tag{7}$$

$$\left.\begin{array}{ll} \text{when } \epsilon_{22} > 0 & \frac{\sigma_{22}-\upsilon_{21}\sigma_{11}-\upsilon_{23}\sigma_{33}}{F_{2t}} \\ \text{when } \epsilon_{22} < 0 & \frac{\sigma_{22}-\upsilon_{21}\sigma_{11}-\upsilon_{23}\sigma_{33}}{-F_{2c}} \end{array}\right\} = 1 \tag{8}$$

$$\left.\begin{array}{ll} \text{when } \epsilon_{33} > 0 & \frac{\sigma_{33}-\upsilon_{31}\sigma_{11}-\upsilon_{32}\sigma_{22}}{F_{3t}} \\ \text{when } \epsilon_{33} < 0 & \frac{\sigma_{33}-\upsilon_{31}\sigma_{11}-\upsilon_{32}\sigma_{22}}{-F_{3c}} \end{array}\right\} = 1 \tag{9}$$

$$\frac{|\sigma_{23}|}{F_4} = 1 \tag{10}$$

$$\frac{|\sigma_{13}|}{F_5} = 1 \tag{11}$$

$$\frac{|\sigma_{12}|}{F_6} = 1 \tag{12}$$

3.3.3. Tsai–Hill's Failure Criterion

The third comparison uses Tsai–Hill's failure criteria [4] which is presented in Eq. (13). The results are shown in Table 8.

$$\frac{\sigma_{11}^2 - \sigma_{11}\sigma_{22} - \sigma_{11}\sigma_{33}}{F_1^2} + \frac{\sigma_{22}^2 - \sigma_{33}^2 - \sigma_{22}\sigma_{33}}{F_2^2} + \frac{\sigma_{23}^2}{F_4^2} + \frac{\sigma_{13}^2 - \sigma_{12}^2}{F_6^2} = 1 \tag{13}$$

3.3.4. Tsai–Wu's Failure Criterion

The fourth comparison uses Tsai–Wu's failure criteria [4] given by Eq. (14). The results are shown in Table 8.

$$H_1\sigma_{11} + H_2\sigma_{22} + H_6\sigma_{12} + H_{11}\sigma_{11}^2 + H_{22}\sigma_{22}^2 + H_{66}\sigma_{12}^2 + 2H_{12}\sigma_{11}\sigma_{22} = 1 \tag{14}$$

where:

$$H_1 = \frac{1}{F_{1t}} - \frac{1}{F_{1c}}$$

$$H_{11} = \frac{1}{F_{1t}F_{1c}}$$

$$H_2 = \frac{1}{F_{2t}} - \frac{1}{F_{2c}}$$

$$H_{22} = \frac{1}{F_{2t}F_{2c}}$$

$$H_6 = 0$$

$$H_{66} = \frac{1}{F_6}$$

Table 3
Critical global strains in the four outer plies of the global model for Specimen 1 (laminate coordinate system).

Ply #	*Fiber direction*	ϵ_{XX} (μ)	ϵ_{YY} (μ)	ϵ_{ZZ} (μ)	*(Engineering)* ϵ_{XY} (μ)	*(Engineering)* ϵ_{XZ} (μ)	*(Engineering)* ϵ_{YZ} (μ)
1	−45	−10100	4960	2010	−2485	3080	590
2	0	−8700	4440	1420	−482	3710	−4200
3	45	−7400	3110	1270	1122	5670	−6900
4	90	−6000	1190	1230	−22	−3600	−100
13	90	6120	−1200	−1200	17	−3900	−100
14	45	7470	−3200	−1200	−1146	5560	−7000
15	0	8860	−4500	−1400	490	3550	−4300
16	−45	10430	−5100	−2100	2629	2580	350

Table 4
Critical local strains in the four outer plies of the global model for Specimen 1 (laminar material coordinate system).

Ply #	*Fiber Direction*	ϵ_{11} (µ)	ϵ_{22} (µ)	ϵ_{33} (µ)	*(Engineering)* ϵ_{12} (µ)	*(Engineering)* ϵ_{13} (µ)	*(Engineering)* ϵ_{23} (µ)
1	−45	−1304	−3789	2013	15018	−1763	2597
2	0	−8708	4443	1422	482	−3711	−4157
3	45	−1564	−2686	1274	−10460	903	−8923
4	90	1195	−6012	1226	−21	−139	−3617
13	90	−1217	6120	−1185	17	−141	−3916
14	45	1584	2729	−1218	10635	998	−8862
15	0	8857	−4520	−1360	−489	−3553	−4283
16	−45	1353	3982	−2055	−15517	−1575	2074

Table 5
Critical failure stresses for EP 280 Prepreg.

	Failure Stress (MPa)	*Method*
F_{1t}	1200	Experiments
F_{1c}	610	Manufacturer
F_{2t}	25	Experiments
F_{2c}	125	Experiments
F_{3t}	25	Experiments
F_{3c}	125	Experiments
F_4	20	Experiments
F_5	60	Experiments
F_6	60	Experiments

$$H_{12} = \frac{1}{2}(H_{11}H_{22})^{1/2}$$

3.3.5. Hashin–Rotem's failure criterion

The final lamina level failure criterion considered is Hashin–Rotem's failure criterion [4] given by Eqs. (15)–(17). This criterion has three conditions to check, if any one of them exceed a value of 1, then failure is predicted. The results are shown in Table 8.

$$\frac{|\sigma_{11}|}{F_1} = 1 \tag{15}$$

$$\left(\frac{\sigma_{22}}{F_2}\right)^2 + \left(\frac{\sigma_{23}}{F_4}\right)^2 + \left(\frac{\sigma_{12}}{F_6}\right)^2 = 1 \tag{16}$$

$$\left(\frac{\sigma_{33}}{F_3}\right)^2 + \left(\frac{\sigma_{23}}{F_4}\right)^2 + \left(\frac{\sigma_{13}}{F_5}\right)^2 = 1 \tag{17}$$

The results presented in Tables 7 and 8 will be discussed in Section 5 of this paper. In Section 5, the matrix failure predictions made at the lamina level are compared to matrix failure predictions made at a micromechanical level using Representative Volume Elements (RVEs). This method is discussed next in Section 4.

4. Method 2: failure at the micro level

Micromechanical analysis is an additional step that can be performed after the lamina level stress/strain states are examined [19,20,25]. Thus, the model of the laminate and the critical stress and strain states obtained in Sections 2 and 3 are still used in the micromechanical level analysis. In order to perform micromechanical analysis, the fiber and matrix are modeled together in a unit cell referred to as a Representative Volume Element (RVE). The authors have used this method in previous investigations [12,13] to obtain a failure criterion for the matrix (EP280) which will be tested for its predictive capability in this section.

The fiber and the matrix are assumed to have isotropic properties given in Table 9 which have been obtained using an inverse method of the rule of mixtures [4]. Where the lamina and matrix properties are used to obtain the fiber properties. 'E' is the Young's Modulus, 'G' is the Shear Modulus, and 'v' is the Poisson's ratio for the material (EP280 Prepreg).

4.1. Finite element analysis

Micromechanical analysis is reliant on finite element analysis (FEA) to extract the individual stress/strain states on the fiber and the matrix. The strain state within the center of the specimen (along path BB) shown in Fig. 4 is extracted for each Ply. These

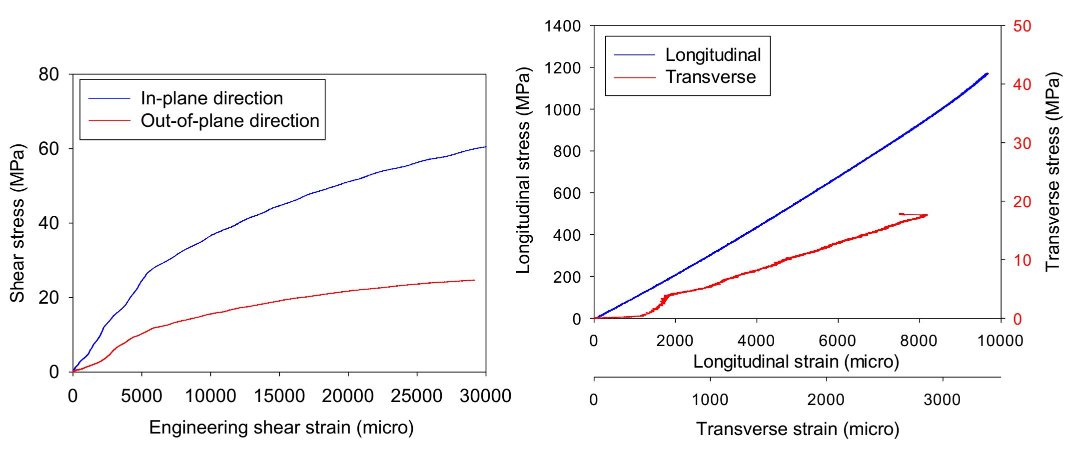

Fig. 6. Material behaviour (EP280 prepreg): (a) nonlinear shear stress/strain relation for EP280 Prepreg, (b) linear stress/strain curve for EP280 Prepreg under longitudinal and transverse tension.

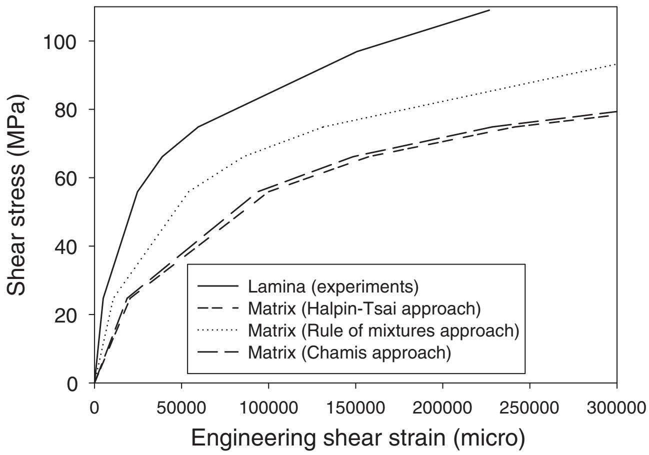

Fig. 7. Nonlinear stress/strain relationship for the lamina and the matrix (EP.280).

Table 6
Critical local stresses in the four outer plies of the global model for Test 1.

Ply #	*Fiber Direction*	σ_{11} (MPa)	σ_{22} (MPa)	σ_{33} (MPa)	σ_{12} (MPa)	σ_{13} (MPa)	σ_{23} (MPa)
1	−45	−170.82	−23.49	12.48	28.64	−4.31	2.75
3	45	−204.88	−16.65	7.90	−25.03	2.21	−9.36
4	90	156.55	−37.27	7.60	−0.05	−0.34	−3.83
13	90	−159.43	37.94	−7.35	0.04	−0.35	−4.15
14	45	207.50	16.92	−7.55	25.17	2.44	−9.30
16	−45	177.24	24.69	−12.74	−29.04	−3.87	2.20

Table 9
Properties for the fibre (calculated) and the matrix (from manufacturer).

Property	*Fibre*	*Matrix*
E	259 GPa	3.140 GPa
G	100 GPa	1.21 GPa
v	0.30	0.30

strain values shown in Table 4 are then applied as displacement boundary conditions onto a RVE with a square fiber configuration. When performing RVE analysis periodic boundary conditions must be maintained [19,20,26] which is difficult to enforce when both normal and shear strains are applied to a single RVE. The authors overcome this by modelling four unit cells for plies 3, 4, 13, and 14. This includes one RVE for the three normal strains and three separate RVEs for each shear strain component (shown in Fig. 8). In previous investigations performed by the authors, the matrix (EP 280) had been predominantly tested under multiaxial tension or compression and a linearly elastic material assumption was found to be appropriate [12,13]. In this paper, the lamina level shear strains shown in Table 4 are found to be nonlinear and also one of the dominant stress cases. Thus it is important that the FEA model correctly models this case.

The laminas nonlinearity is shown in Fig. 6a. it is important that this lamina level nonlinearity is also reflected in its constituents. In order to do this, three numerical micromechanical models are compared: Rule of Mixtures [4], Halpin-Tsai's equation [4] and Chamis's equation [27] (given by Eqs. (18)–(20) respectively). The authors assume the fiber to behave in a linear isotropic manner, whilst the matrix is treated as an isotropic material which behaves linearly in the materials normal directions, but

Table 7
Summary of failure predictions using the Maximum Stress and Maximum Strain failure criteria, expressed as failure index. (Red: indicates failure, yellow: indicates close to failure).

	Ply #	*Fiber Direction*	σ_{11}	σ_{22}	σ_{33}	σ_{12}	σ_{13}	σ_{23}
Maximum Stress failure criteria	1	-45	0.28	0.19	0.50	0.48	-0.07	0.14
	3	45	0.34	0.13	0.32	-0.42	0.04	-0.47
	4	90	0.13	0.30	0.30	0.00	-0.01	-0.19
	13	90	0.26	1.52	0.06	0.00	-0.01	-0.21
	14	45	0.17	0.68	0.06	0.42	0.04	-0.47
	16	-45	0.15	0.99	0.10	-0.48	-0.06	0.11
Maximum Strain failure criteria	1	-45	0.27	0.21	0.97	0.48	-0.07	0.14
	3	45	0.33	0.14	0.69	-0.42	0.04	-0.47
	4	90	0.14	0.34	0.82	0.00	-0.01	-0.19
	13	90	0.28	1.72	0.16	0.00	-0.01	-0.21
	14	45	0.17	0.69	0.14	0.42	0.04	-0.47
	16	-45	0.14	1.10	0.20	-0.48	-0.06	0.11

Table 8
Summary of failure predictions given by: Tsai–Hill's, Tsai–Wu's, and Hashin–Rotem's failure criteria, expressed as failure index. (Red: indicates failure).

Ply #	*Fiber Direction*	*Tsai-Hill*	*Tsai-Wu*	*Hashin-Rotem*		
				condition 1	*condition 2*	*condition 3*
1	-45	0.39	-0.25	-0.28	0.28	0.27
3	45	0.53	-0.12	-0.34	0.41	0.32
4	90	0.17	-0.72	0.13	0.13	0.13
13	90	2.96	1.96	-0.26	2.35	0.05
14	45	1.18	0.63	0.17	0.85	0.22
16	-45	2.01	1.03	0.15	1.22	0.03

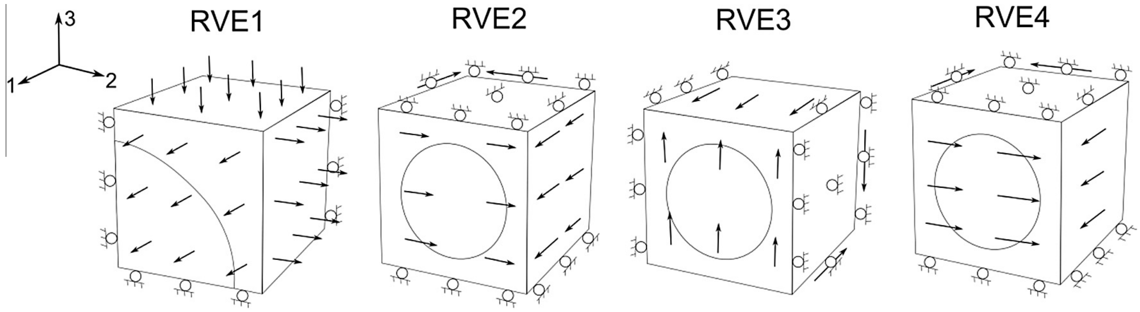

Fig. 8. RVE (square fiber configuration) with boundary conditions applied.

Table 10
Elastic shear modulus prediction given by three different micromechanical models.

	G_m (GPa)	*Percentage difference from experiment value*
Experiment	1.21	NA
Rule of mixtures	2.27	88%
Halpin-Tsai	1.21	0%
Chamis	1.32	9%

nonlinearly in its shear directions. A plot of the matrix nonlinear relationship using Eqs. (18)–(20) is shown in Fig. 7.

$$\frac{1}{G_{12}} = \frac{v_f}{G_f} + \frac{(1 - v_f)}{G_m} \tag{18}$$

$$G_{12} = \frac{G_m(1 + \xi\eta v_f)}{\eta v_f} \quad where\ \eta = \frac{\left(\frac{G_f}{G_m} - 1\right)}{\left(\frac{G_f}{G_m} + \xi\right)} \tag{19}$$

$$G_{12} = \frac{G_m}{1 - \sqrt{v_f}(1 - \frac{G_m}{G_f})} \tag{20}$$

where:
ξ: calibration factor,
G_{12}: shear modulus of the lamina,
G_m: shear modulus of the matrix
G_f: shear modulus of the fiber,
v_f: fiber volume fraction.

From the three micromechanical models compared, Table 10 shows the prediction of the laminas initial elastic shear modulus. It can be seen that the Rule of mixtures over predicts the shear modulus, whilst the Halpin-Tsai and Chamis models were able to predict the shear modulus to within 10% accuracy. For the Halpin-Tsai model, this accuracy is expected as the model has a calibration factor to improve its prediction, on the other hand the Chamis model has no calibration factors and is able to maintain a good elastic shear modulus prediction (difference of 9%). For this

Table 11
Principal stresses on the matrix for a square fiber configuration RVE (Test 1).

Ply #	*Fiber Direction* (Degrees)	σ_1 (MPa)	σ_2 (MPa)	σ_3 (MPa)
1	+45	17.21	−125.52	−29.65
2	0	50.88	−15.91	−5.33
3	−45	20.01	−104.30	−23.17
4	90	−31.47	−110.03	−38.67
13	90	112.14	31.88	39.36
14	−45	116.12	−32.05	25.24
15	0	16.25	−51.69	5.62
16	+45	128.33	−14.18	31.21

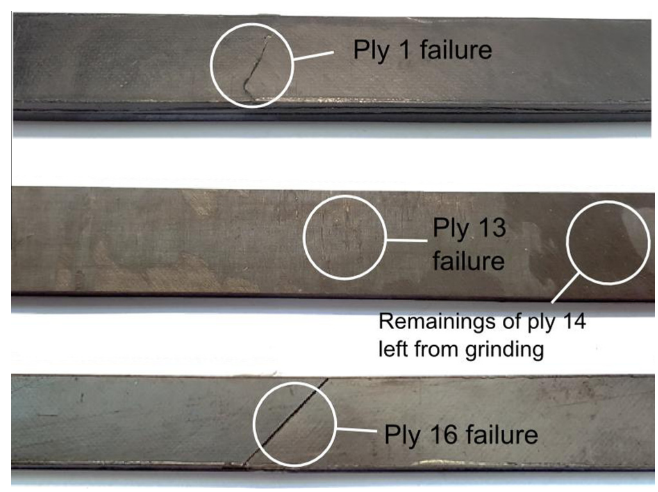

Fig. 10. Failure observed in specimens after post-failure inspection.

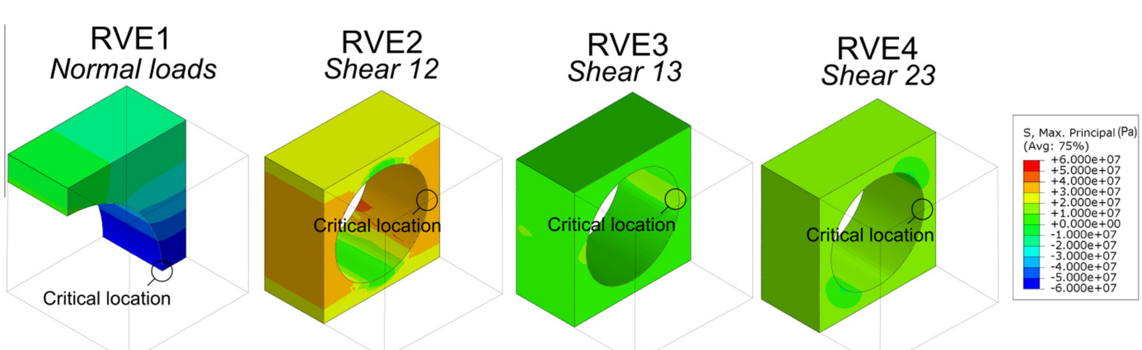

Fig. 9. Example of the critical location selected for a square RVE (Specimen 1, Ply 3).

Table 12
Principal stresses on Ply 3 and Ply 13 for the matrix. (Average of four fiber configurations.)

Test #	*Ply #*	σ_1 (MPa)	σ_2 (MPa)	σ_3 (MPa)
1	3	33.53	−91.01	−18.04
2	3	37.78	−91.88	−17.48
3	3	36.45	−91.88	−17.92
4	3	36.99	−88.15	−16.46
5	3	37.25	−103.77	−21.44
6	3	37.02	−107.33	−22.68
7	3	37.07	−89.44	−16.84
8	3	37.31	−91.76	−17.50
Average	3	36.68	−94.40	−18.55
1	13	86.28	12.56	25.81
2	13	81.27	11.77	24.32
3	13	83.77	12.20	25.07
4	13	76.68	11.16	22.95
5	13	100.35	14.58	30.01
6	13	106.16	15.62	31.81
7	13	78.68	11.39	23.49
8	13	81.81	11.86	24.45
Average	13	86.88	12.64	25.99

Table 13
Comparison of processed experiment results for Ply 3 with the Drucker–Prager failure criterion. (Red: indicates failure, yellow: indicates close to failure).

Test	*Ply #*	*Drucker-Prager failure index (Eq. 22):*
1	3	0.94
2	3	0.98
3	3	0.97
4	3	0.95
5	3	1.05
6	3	1.07
7	3	0.96
8	3	0.97

reason, the Chamis micromechanical model is selected as the basis of modeling the shear nonlinearity of the matrix (EP280). A user material subroutine (UMAT) was written for ABAQUS 6.13 to implement anisotropic nonlinear material behavior.

After displacement boundary conditions are applied using the critical strains obtained in each ply of the specimen on the RVEs (shown in Fig. 8), the UMAT is run. Each RVE is then probed at their critical location shown in Fig. 9 and superimposed according to Eq. (21).

$$\begin{Bmatrix} S^s_{11} \\ S^s_{22} \\ S^s_{33} \\ S^s_{12} \\ S^s_{23} \\ S^s_{13} \end{Bmatrix} = \begin{Bmatrix} S^{RVE1}_{11} \\ S^{RVE1}_{22} \\ S^{RVE1}_{33} \\ S^{RVE1}_{12} \\ S^{RVE1}_{23} \\ S^{RVE1}_{13} \end{Bmatrix} + \begin{Bmatrix} S^{RVE2}_{11} \\ S^{RVE2}_{22} \\ S^{RVE2}_{33} \\ S^{RVE2}_{12} \\ S^{RVE2}_{23} \\ S^{RVE2}_{13} \end{Bmatrix} + \begin{Bmatrix} S^{RVE3}_{11} \\ S^{RVE3}_{22} \\ S^{RVE3}_{33} \\ S^{RVE3}_{12} \\ S^{RVE3}_{23} \\ S^{RVE3}_{13} \end{Bmatrix} + \begin{Bmatrix} S^{RVE4}_{11} \\ S^{RVE4}_{22} \\ S^{RVE4}_{33} \\ S^{RVE4}_{12} \\ S^{RVE4}_{23} \\ S^{RVE4}_{13} \end{Bmatrix} \tag{21}$$

Once the stresses are obtained from Eq. (21), they are converted to principal stresses. Due to the random packing of fibers within a lamina, four fiber configurations are analyzed for each failure point. They include the square, diamond, horizontal hexagonal and vertical hexagonal fiber configurations shown in Fig. 9. 1024 simulations would need to be run in total for the 8 specimens tested, where each of the four outer plies (plies 1–4, 13–16) were analyzed using RVEs which included normal and shear loads and four different fiber configurations. To reduce this number by a fifth, only one fiber configuration (square) was initially analyzed for all the plies in Test 1. Then based on observed failure locations in our experiments; plies 3 and 13 were analyzed in more detail for the remainder specimen tests.

4.2. Results

The processed results for the square fiber configuration RVE using 'Test 1' experimental results are recorded in Table 11. Where σ_1, σ_2, and σ_3 are the three principal stresses.

Post inspection of the specimens revealed that plies 1, 3, 13, and 16 have failed. Ply 3 failure was picked up by the FLIR thermal camera. However it should be noted that the FLIR thermal camera is only able to pick up failure on the specimen facing the camera and does not necessarily indicate whether other plies have also failed. Failure of plies 1 and 16 was visible from post inspection of all the specimens although they were not observed to fail throughout the load regime indicating that failure had occurred before Ply 3 but undetected. Ply 1 failure demonstrated signs of fiber kinking, which is a known characteristic resulting from matrix shear [24]. To inspect matrix failure on the inner plies a diamond wheel was used to grind each Ply off one at a time. On Specimens 1, 5, and 6 cracks were visible on Ply 13 indicating matrix failure, whilst on the other specimens, no clear matrix cracks were observed. This may be indicative that the other specimens may have been on the verge of failure. Pictures of the specimens during post-failure inspection are shown in Fig. 10.

For these reason the authors have decided to focus the remainder of this investigation on Ply 13 and Ply 3. Table 12 summarises the stress state at failure for the matrix for all eight of the experiments. The principal stresses shown are the average of four fiber configurations tested: square, diamond, horizontal hexagonal, and vertical hexagonal configurations discussed earlier.

Table 14
Comparison of processed experimental results of Ply 13 with the 1st Stress Invariant. (Red: indicates failure, yellow: indicates close to failure).

Test	*Ply #*	*Failure index when J_1 =167.5*	*Failure index when J_1 =120.4*	*Failure index when J_1 =153.2*
1	13	0.74	1.04	0.81
2	13	0.70	0.97	0.77
3	13	0.72	1.01	0.79
4	13	0.66	0.92	0.72
5	13	0.87	1.20	0.95
6	13	0.92	1.28	1.00
7	13	0.68	0.94	0.74
8	13	0.71	0.98	0.77

4.3. Failure prediction at the micro level

In previous investigations performed by the authors [12,13,28], the material being tested (EP280) was designed so that failure points for the matrix could be obtained from which a failure criterion for the matrix was recommended. In this investigation the authors wish to verify the accuracy of the failure criterion by performing tests on a typical laminate stacking found in composite structures. The authors had found that the Drucker–Prager failure criterion best predicts compressive and shear modes of failure for the matrix material (EP 280) used in this study [13]. The obtained failure criterion for EP 280 is presented as a failure index in Eq. (22). The authors had also found from biaxial tensile tests performed on a FRPC specimen, that all the tensile failure results fell on the 1st Stress Invariant given by Eq. (24) [19,29,30]. The failure index values obtained using Eqs. (22) and (24) are shown in Tables 13 and 14. Matrix failure is predicted when Eqs. (22) and (24) are greater than 1. The 1st Stress Invariant was found by performing biaxial tensile tests on three different types of specimens; (1) fiber reinforced specimens where J_1 was found to be equal to 167.5 MPa. (2) Uniaxial off-axis tensile tests on fiber reinforced specimens (J_1 = 120.4 MPa). (3) Biaxial tensile tests on a neat resin specimen made of the same matrix material where J_1 was found to be equal to 153.2 MPa.

$$\frac{\sqrt{J_2}}{62.25 - 0.061(\sigma_1 + \sigma_2 + \sigma_3)} = 1 \tag{22}$$

where:

$$J_2 = \frac{1}{6}\left[(\sigma_1 - \sigma_2)^2 + (\sigma_2 - \sigma_3)^2 + (\sigma_3 - \sigma_1)^2\right] \tag{23}$$

σ_1, σ_2, and σ_3 are the principal stresses in the fiber, transverse and out-of-plane directions respectively.

J_1 is the 1st Stress Invariant.

$$\frac{\sigma_1 + \sigma_2 + \sigma_3}{J_1} = 1 \tag{24}$$

The failure results from the four point bend tests are plotted on the previously obtained Drucker–Prager failure surface and the 1st Stress Invariant. This is shown in Fig. 11.

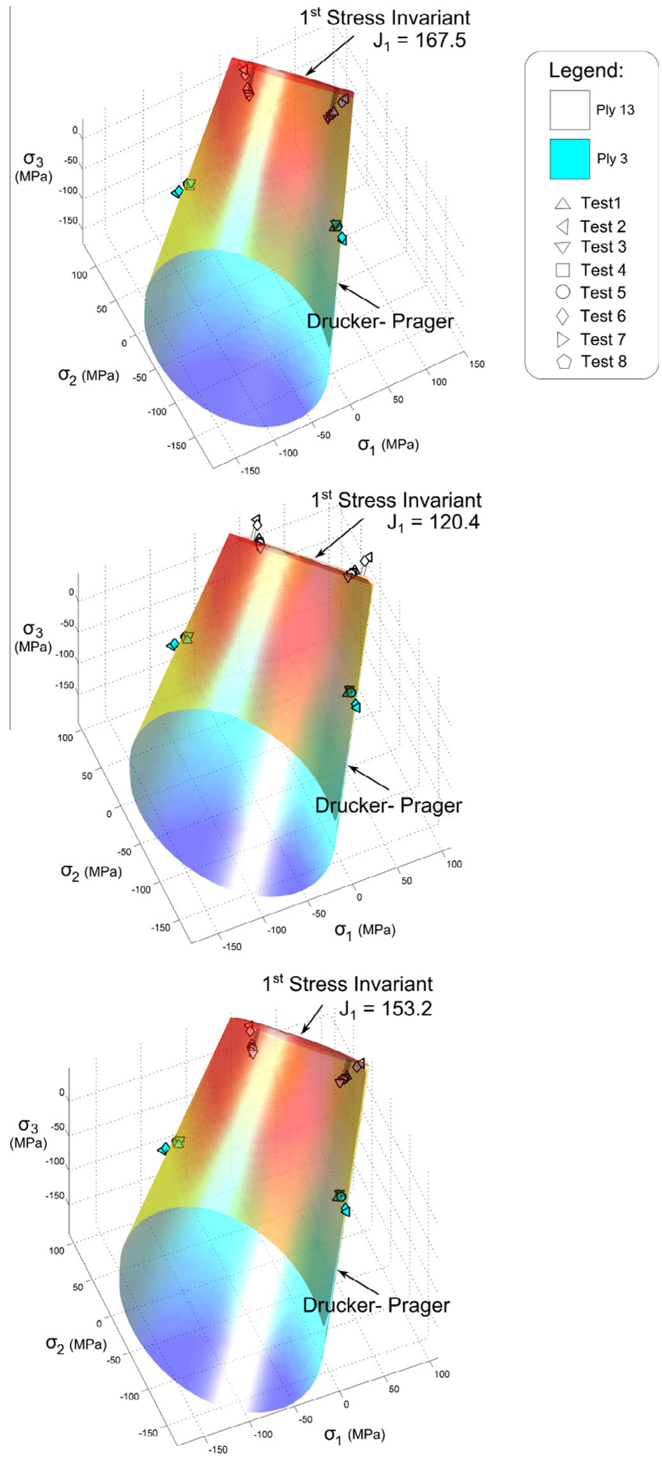

Fig. 11. Plot of processed failure results on the previously obtained Drucker–Prager and 1st Stress Invariant [9].

5. Overall discussion

The results for matrix failure prediction at the lamina level are compared against the matrix failure prediction obtained by the authors at a micro level. Table 15, summarises the results for specimen 1 discussed in those sections. For completeness of data the readers may refer to the original tables in Sections 2 and 3 of this paper.

The values in Table 15 are presented in failure index form (FI) where a value of 1 or more indicates failure to have taken place, these values are also highlighted in red. As discussed in Section 3 and shown in Fig. 10, post inspection of the specimens revealed plies 1 and 16 (the two outer plies) to have failed sometime early on in the loading regime. From Table 15 it can be seen that the maximum strain failure theory predicts failure about to take place (FI = 0.97) whilst all the other lamina level failure criteria suggest that no failure has taken place, thus over predicting failure. The hybrid criterion used by the authors in the micromechanical analysis was the only failure criterion that correctly predicted failure to have taken place early on in the loading regime (FI = 1.03). Looking at the FI values for Ply 16; we can generally say that all the lamina level failure criteria predicted failure to have taken place. However the spread in their predictions is quite large with Tsai–Wu predicting failure (FI = 1.03) taking place slightly earlier than when the experiments were stopped, whilst Tsai–Hill failure criterion predicted failure to take place (FI = 2.01) at almost half way into the loading regime. Micromechanical analysis using the proposed failure criterion did also predict failure with an FI value of 1.36 which generally falls in the mean of the spread given using the lamina level failure criteria. Validation of which criterion is most accurate cannot be made as the time at failure for Ply 16 was not observed but overall it can be said that all failure criteria did correctly predict failure to have occurred. Ply 3 is the most important to

Table 15
Summary of matrix failure predictions at the lamina and micro level (using Specimen 1 results). (Red: indicates failure, yellow: indicates close to failure).

Ply #	Fiber Direction	Failure at the lamina level					Failure at the micro level
		Max Stress	Max Strain	Tsai-Hill	Tsai-Wu	Hashin-Rotem (Condition 2)	Drucker-Prager & 1st Stress Invariant Hybrid (J_1=120.4)
1	-45	0.5 (σ_{33})	0.97 (σ_{33})	0.39	-0.25	0.28	1.03
3	**45**	**-0.47 (σ_{23})**	**0.69 (σ_{33})**	**0.53**	**-0.12**	**0.41**	**0.94**
4	90	-0.30 (σ_{22})	0.82 (σ_{33})	0.17	-0.72	0.13	0.59
13	**90**	**1.52 (σ_{22})**	**1.72 (σ_{22})**	**2.96**	**1.96**	**2.35**	**1.04**
14	45	0.68 (σ_{22})	0.69 (σ_{22})	1.18	0.63	0.85	1.34
16	-45	0.99 (σ_{22})	1.10 (σ_{22})	2.01	1.03	1.22	1.36

consider from the experiments, as the time at failure was observed using the FLIR thermal camera and post-inspection had also revealed matrix failure in this Ply. Using Table 15, all the lamina level failure criteria did not predict failure with the closest being predicted by Maximum Strain failure criterion which suggested that the specimen was 69% of the way to failure (FI = 0.69). On the other hand, the micromechanical hybrid failure criterion proposed by the authors gave the best prediction of FI = 0.94. Thus with a 6% error it can be said that this model was able to capture matrix failure in Ply 3. The final Ply that was inspected for damage was Ply 13. Ply 13 is of particular interest to the authors due to two reasons. The first is due to that fact that in 'Method 1' all the failure criteria discussed predicted that Ply 13 had failed. This can be also seen in Table 15. The second reason is that Ply 13 is found to experience a triaxial tensile stress state (although close to being in shear) (Table 11). This particular mode of failure has been examined in detail by the authors in previous studies [12], where it was found that matrix failure was best predicted using the 1st Stress Invariant failure criterion. From Table 14 and Fig. 11 it can be seen that the failure observed in Ply 13 (under triaxial tension) does cluster around the proposed failure surface. With the best prediction given when the 1st stress invariant (J_1) is equal to 120.4, giving a difference of 4% (average) between the processed experimental results and the proposed failure model.

The lamina level failure criteria all correctly predicted Ply 13 failure for specimen 1, however their failure index values range from 1.53 to 2.96 given by Maximum Stress and Tsai–Hill failure criteria respectively. This implies that all the lamina level failure criteria predict failure to have occurred earlier than the time at which these results have been analyzed, where a value of F1 = 2.96 suggests failure to have occurred very early in the loading regime. Although no specific time at failure was observed for Ply 13 we assume that it occurs around the time at which the loading regime was stopped, as specimens 1, 5, and 6 shown in Table 12 were found to have failed whilst all the other specimens tested had not. Thus the micromechanical analysis using the 1st Stress Invariant still gave the best failure prediction with an FI value of 1.04.

The results presented here demonstrate the success in using micromechanical analysis to predict matrix failure in composite structures. Eq. (25) is now proposed which builds on the concept proposed by Gosse and Christensen [20] when they presented Strain Invariant Failure Theory (SIFT). In this paper the authors suggest a hybrid formulation which uses Drucker–Prager failure criterion to predict compressive and shear dominant failure in composite structures due to the matrix. Whilst using the 1st Stress Invariant is found to predict triaxial tensile failure the best.

$$\text{Matrix failure occurs if}: \begin{cases} \sigma_1+\sigma_2+\sigma_3 \geqslant X_t, \quad \textit{where} \quad \sigma_1,\sigma_2,\&\sigma_3 \geqslant 0 \\ \textit{else}: \\ \sqrt{\frac{1}{6}[(\sigma_1-\sigma_2)^2+(\sigma_2-\sigma_3)^2+(\sigma_3-\sigma_1)^2]} \geqslant A - B(\sigma_1+\sigma_2+\sigma_3) \end{cases} \tag{25}$$

where:

σ_1, σ_2, and σ_3 are the principal stresses.
X_t is the uniaxial tensile strength of the matrix material.
'A', and 'B' are curve fitting parameters obtained for the Drucker–Prager failure criterion using matrix data.

6. Conclusions

Matrix failure was observed in the composite specimen tested. It was found that matrix failure was best observed through the use of a FLIR thermal imaging camera. Other detection methods such as the load–displacement curve and visual inspection throughout the tests were not as conclusive. The limitation of failure detection using the FLIR thermal camera is that failure on the exposed faces of the specimen can only be detected. Matrix failure in Ply 3 was picked up clearly by the thermal camera and its time at failure was used as the basis for analyzing all the experiments. Post inspection of the specimens revealed Ply 13 to be on the verge of failure as 3 out the 8 specimens tested had shown signs of matrix failure when the outer layers were removed using a diamond wheel.

Failure predictions at the lamina and micro level were performed which revealed micromechanical analysis to do a much better job in capturing matrix failure. At the lamina level, none of the five failure criteria investigated were able to predict Ply 3 failure. Whilst all of them over predicted Ply 13 failure by at least

52% with the worst over predicting by nearly 200%. Ply 3 and Ply 13 failure were best captured at the micromechanical level to within 6% and 4% respectively for Specimen 1. The authors suggest the use of a hybrid failure criterion comprised of the Drucker–Prager failure criterion to predict matrix compressive and shear failure, whilst the 1st Stress Invariant is suggested for use in matrix tensile failure cases.

Acknowledgments

This work was undertaken as part of a CRC-ACS research program, established and supported under the Australian Government's Cooperative Research Centres Program.

Dr Nik Rajic (DSTG) for the use of MiTE thermal imaging software.

Leslie Wong (PhD student at Monash University) for assistance and processing in the use of fiber optic strain measurements.

References

[1] Welsh Jeffry S, Mayes JS, Key Christopher T, Mclaughlin Richard N. Comparison of MCT failure prediction techniques and experimental verification for biaxially loaded glass fabric-reinforced composite laminates. J Compos Mater 2004;38:2165–81.
[2] Reddy JN. Mechanics of laminated composite plates and shells: theory and analysis. 2nd ed. Taylor & Francis; 2004.
[3] Helius: MCT Technical Manual Version 1.0 ed. 2009, Firehole Technologies.
[4] Daniel IM, Isha O. Engineering mechanics of composite materials. Oxford University Press; 2006.
[5] Girão Coelho Ana M, Mottram JT, Harries Kent A. Finite element guidelines for simulation of fibre-tension dominated failures in composite materials validated by case studies. Compos Struct 2015;126:15.
[6] Wind JL, Waas AM, Jensen HM. Initiation of failure at notches in unidirectional fiber composites. Compos Struct 2015;122:51–6.
[7] Lee C-S et al. Initial and progressive failure analyses for composite laminates using Puck failure criterion and damage-coupled finite element method. Compos Struct 2015;121:406–19.
[8] Su ZC et al. Progressive damage modeling of open-hole composite laminates under compression. Compos Struct 2015;122:507–17.
[9] Wang L et al. Continuum damage modeling and progressive failure analysis of carbon fiber/epoxy composite pressure vessel. Compos Struct 2015;134:475–82.
[10] Zhang J et al. A progressive damage analysis based characteristic length method for multi-bolt composite joints. Compos Struct 2014;108:915–23.
[11] Aidi Bilel, Philen MK, Case Scott W. Progressive damage assessment of centrally notched composite specimens in fatigue. Compos Part A 2015;74:47–59.
[12] Chowdhury NT et al. Matrix failure in composite laminates under tensile loading. Compos Struct 2016;135:61–73.
[13] Chowdhury NT. Matrix failure in composite laminates under compressive loading. Compos Part A (in press).
[14] GMS Composites Standard Prepreg Range & Technical datasheets (EP 280). [cited 2015 October 1]; Available from: <http://www.gmscomposites.com/prepreg-range/prepreg-technical-datasheets/>.
[15] ASTM D7264 – Standard test method for flexural properties of polymer matrix composite materials; 2007.
[16] Lim K et al. Distributed fiber optic sensors for monitoring pressure and stiffness changes in out-of-round pipes. Struct Control Health Monit. 2015.
[17] Lammens N et al. Finite element prediction of resin pocket geometry around embedded optical fiber sensors in prepreg composites. Compos Struct 2015;132:825–32.
[18] Hibbit Karlsson. A.B.A.Q.U.S./Sorensen Standard Analysis User's Manual. Hibbit, Karlsson: Sorensen Inc; 2014.
[19] Hart-Smith LJ. Application of the strain invariant failure theory (SIFT) to metals and fiber–polymer composites. Philos Mag 2010;90(31–32):4263–331.
[20] Gosse JH, Christensen S. Strain invariant failure criteria for polymers in composite materials; 2001.
[21] ASTM D3039 – Standard test method for tensile properties of polymer matrix composite materials; 2008.
[22] ASTM D695 – Standard test method for compressive properties of rigid plastics; 2015.
[23] ASTM D5379 – Standard test method for shear properties of composite materials by the V-Notched beam method; 2012.
[24] Szekrényes A, Jozsef Uj. Finite element modelling of the damage and failure in fiber feinforced composites (overview). Periodica Polytechnica Ser. Mech Eng 2002;46(2):139–58.
[25] Tran T et al. A micromechanical sub-modelling technique for implementing onset theory. Compos Struct 2013;103:1–8.
[26] Gosse, R.B.P.A.J.H., An onset theory for irreversible deformation in composite materials; 2010.
[27] Younes R et al. Comparative review study on elastic properties modeling for unidirectional composite materials. INTECH Open Access Publisher; 2012.
[28] Chowdhury NT, Wang J, Chiu WK. Design of a flat plate specimen suitable for biaxial tensile tests on polymer materials. Polym Polym Compos 2015;23(9):627–38.
[29] Gosse John H. Strain invariant failure criteria for polymers in composite materials. American Institute of Aeronautics and Astronautics; 2001. p. 11.
[30] Hart-Smith L. Mechanistic failure criteria for carbon and glass fibers embedded in polymer matrices. Am Inst Aeronaut Astronaut 2001;1(2001–1183):34–44.